Article Title: Overexpression of Rubisco subunits with RAF1 increases Rubisco content in maize

Authors and Affiliations:

Coralie Salesse[1], Robert Sharwood[2], Florian A. Busch[2], Johannes Kromdijk[3], Viktoriya Bardal[1] and David Stern[1*]

Boyce Thompson Institute, Cornell University, Ithaca, New York, 14853, USA (C.S., D.S.)[1]; Research School of Biology, The Australian National University, Canberra, ACT, 2601, Australia (R.S., F.B)[2] and Carl R. Woese Institute for Genomic Biology, University of Illinois, 1206 West Gregory Drive, Urbana, IL 61801, USA (J.K)[3]

Abstract

Rubisco catalyzes a rate-limiting step in photosynthesis and has long been a target for improvement due to its slow turnover rate. An alternative to modifying catalytic properties of Rubisco is to increase its abundance within C_4 plant chloroplasts, which might increase activity and confer a higher carbon assimilation rate. Here, we overexpress the Rubisco large (LS) and small (SS) subunits with the Rubisco assembly chaperone RAF1. While overexpression of LS and/or SS had no discernable impact on Rubisco content, addition of RAF1 overexpression resulted in a >30% increase in Rubisco content. Gas exchange showed a 15% increase in CO_2 assimilation (A_{SAT}) in UBI-LSSS-RAF1 transgenic plants, which correlated with increased fresh weight and *in vitro* V_{cmax} calculations. The divergence of Rubisco content and assimilation could be accounted for by the Rubisco activation state, which decreased up to 23%, suggesting that Rubisco activase may be limiting V_{cmax}, and impinging on the realization of photosynthetic potential from increased Rubisco content.

Most life hinges on the ability of photosynthetic organisms to convert atmospheric CO_2 into organic compounds. The enzyme that catalyzes the rate-limiting step in this reaction is Ribulose-1,5-bisphosphate carboxylase/oxygenase (Rubisco), a major target for improvement due to its slow turnover rate and poor substrate affinity (1). Form I Rubisco is found in plants, algae and cyanobacteria, and is a 550 kD hexadecamer composed of 8 small subunits (SS) encoded by the nuclear *RBCS* gene family, and 8 large subunits (LS) encoded by the chloroplast gene *rbcL*. These subunits are assembled through a pathway best described in cyanobacteria (2), which is likely to be generally applicable to plants, as discussed below.

Rubisco is catalytically slow, and is subject to a competing oxygenation reaction that leads to photorespiration, which is energetically wasteful under most conditions through the loss of previously fixed CO_2. C_3 plants circumvent this problem by investing significant amounts of nitrogen into Rubisco synthesis to attain appreciable rates of CO_2 assimilation. However, in C_4 plants, the allocation of nitrogen to Rubisco is much less due to the operation of a CO_2 concentrating mechanism (CCM) that relies on biochemical and anatomical adaptations (Kranz anatomy) to differentially compartmentalize the two carboxylases PEPC (phosphoenolpyruvate carboxylase) and Rubisco. In C_4 plants, Rubisco is localized within the bundle sheath (BS) chloroplasts, where its efficiency is improved by this CCM which instills a high CO_2 environment relative to mesophyll (M) chloroplasts and the atmosphere. This CCM operates through initial fixation of HCO_3^- by PEPC in M chloroplasts to convert three carbon PEP to a four-carbon compound (C_4 cycle), that diffuses into the BS and is decarboxylated to produce pyruvate and release high levels of CO_2 around the active sites of Rubisco (C_3 Cycle). PEP is regenerated through pyruvate inorganic phosphate dikinase (PPDK) which catalyzes the ATP/Pi-dependent conversion of pyruvate to PEP. PPDK, along with Rubisco, is believed to limit CO_2 assimilation in C_4 plants (3).

The CCM within BS cells has led Rubisco to evolve a higher catalytic rate (4, 5) and conferred the ability to operate at its maximum speed. This improves the tolerance of C_4 plants to heat and drought through better water use efficiency, while reducing the N budget to 4-9% of total leaf N, in contrast to the 20-30% of leaf N content allocated to Rubisco in C_3 plants (6). In order to raise the CO_2 concentration in the BS, the C_4 cycle operates faster than the C_3 cycle. The rate at which the fraction of concentrated CO_2 not fixed by Rubisco leaks back into the M cells relative to the rate of PEP carboxylation, is termed leakiness (Φ; 7). It is important for C_4 plants to maintain a balance between the C_3 and C_4 cycles to minimize BS leakiness. Due to the energetic expense to concentrate CO_2 via the C_4 cycle, excessive Φ is considered a wasteful process as a result of the additional ATP required to re-fix CO_2 that diffuses back to the M (8).

There have been numerous efforts to alter Rubisco properties or expression to improve photosynthesis, including mutagenesis and subunit swapping to alter catalytic properties (reviewed in 9). Another strategy, used in rice, was to increase Rubisco content through overexpression of *RBCS*. While this resulted in a maximal 30% increase in Rubisco content, no corresponding improvement to photosynthetic rate was observed either at high or low CO_2 concentrations, for reasons that remain unclear (10). We previously attempted a similar approach in maize, but failed to observe increased Rubisco content in transgenic lines overexpressing SS or a combination of SS and LS, with the latter ectopically expressed from the

nucleus with a chloroplast transit peptide (11). These results suggested that to increase Rubisco content, assembly and/or stability factors needed to be considered. In maize, mutant data have identified four chaperones that are required for Rubisco assembly and seedling survival. These are the Cpn60α1 (GroEL homologue) CPS2 (12), Bundle Sheath Defective2 (BSD2), a small Zn-finger containing protein (13), and the novel proteins Rubisco Assembly Factor 1 (RAF1) and Rubisco assembly factor 2 (RAF2) (14, 15). The roles of RAF1, CPS2 and BSD2 have been recently defined through bacterially-mediated assembly of Arabidopsis Rubisco (16), while the precise role of RAF2 remains enigmatic. RbcX, which has been structurally studied in Arabidopsis (17), is also required for *in vitro* assembly.

BSD2 participates in the final exchange of SS onto LS octamers *in vitro* (16). A cyanobacterial homologue of RAF1 has been shown to stabilize LS dimers in cyanobacterial Rubisco assembly (18), and the co-expression of Arabidopsis RAF1 with Arabidopsis LS and native SS in tobacco chloroplasts, greatly improved assembly (19). RAF2 function is less well understood, but it has been shown to promote Rubisco assembly in a heterologous bacterial system (20), as well as in the Arabidopsis *in vitro* system (16). Rubisco performance also depends on the AAA+ ATPase Rubisco activase (RCA). RCA generates a conformational change leading to removal of inhibitory sugar phosphates from the Rubisco catalytic site (21), and is also a target for improvement due to its poor performance under certain abiotic stress conditions (22).

We hypothesized that in maize, a C_4 plant, nitrogen allocation to Rubisco is sufficiently low that a net gain in photosynthetic performance might be realized if Rubisco content could be increased. To test this hypothesis, we developed transgenic maize designed to overexpress Rubisco subunits in combination with RAF1. We report that both Rubisco protein content and activity could be improved, and could be correlated with increased plant growth.

Results

Transgenic maize with increased Rubisco abundance

The three transgenes shown in Figure 1a were used in the experiments reported here. Each contains the maize ubiquitin promoter (constitutively expressed in M and BS), the maize coding sequence of interest, and the Nos 3' terminator. Each transgene was stably introduced into Hi-II maize, and multiple single-insertion, non-silencing events were propagated. Lines overexpressing the Rubisco subunits (UBI-LSSS and UBI-SS) were reported previously (11), and it was found that LS expressed from the nucleus, with a Flag epitope tag, accounted for 20-60% of the LS incorporated into Rubisco holoenzyme. No Rubisco, however, was found to accumulate in mesophyll cells, where the transgenes are also expressed. Protein expression, photosynthesis and plant growth of three independent transgenic events for the new UBI-RAF1 overexpression lines were initially characterized (Figure S1). No significant differences were observed, and a representative event was chosen for genetic crosses and further analyses. Homozygous lines were crossed to Hi-II or each other (e.g. UBI-RAF1 x Hi-II, UBI-RAF1 x UBI-LSSS) to create hemizygotic F1 plants, which were used as experimental material.

107 As experimental controls, we compared Hi-II plants – the transformation recipient – as well as
108 wild-type (WT) siblings segregating in crosses involving UBI-RAF1 or UBI-LSSS-RAF1, and Hi-
109 II. Because the photosynthesis, protein expression and plant growth data obtained from these
110 two types of controls were statistically indistinguishable (Figure S2), Hi-II was chosen as the
111 non-transgenic control and is referred to as WT.

112 Co-overexpression of Rubisco assembly factor 1 and Rubisco subunits results in increased
113 Rubisco holoenzyme in BS chloroplasts

114 Analysis of Rubisco content in transgenic lines was performed using a ^{14}C-CABP binding assay.
115 Statistically significant increases of 36% and 33% were observed in the UBI-SS-RAF1 and UBI-
116 LSSS-RAF1 lines, respectively (Figure 1b). We also confirmed that overexpression of LS and
117 SS alone did not lead to increased Rubisco content. Finally, a small increase in Rubisco content
118 was observed for UBI-RAF1.

119 We investigated whether all Rubisco was accumulating in BS cells, using cell type separation
120 and immunoblotting with BS and M-specific markers (Figure 1c). As expected, no Rubisco was
121 detected above contaminant levels in M preparations, as judged by marker proteins. Then,
122 native protein preparations were analyzed by immunoblot to assess whether all accumulating
123 Rubisco subunits were present in the L_8S_8 holoenzyme. When probed for LS using either anti-
124 LS or anti-Flag, only the 550 kD holoenzyme was observed (Figure 1d). Specifically, other parts
125 of the gels where either smaller LS-containing complexes, or larger intermediates not yet
126 containing SS would migrate, showed no observable signal. This was expected since Rubisco
127 assembly intermediates are thought to be highly unstable and/or of low abundance. The
128 significant overexpression of RAF1 in UBI-RAF1 lines is also evident in Figure 1d.

129 Increased Rubisco abundance is correlated with increased activity and decreased activation
130 state

131 Increased Rubisco content does not necessarily translate to increased activity, therefore we
132 assessed activity present in leaf extracts, and activation state. Total Rubisco activity (i.e. fully
133 activated enzyme) was increased in lines overexpressing RAF1 (Figure 2a), with UBI-RAF1 and
134 UBI-LSSS-RAF1 showing significant increases. Regression analysis showed a correlation
135 between Rubisco content and activity (r^2=0.81, Figure 2b). This suggests that there is not a
136 substrate limitation in the higher abundance lines. When Rubisco activation state (i.e. the
137 fraction of catalytically competent Rubisco active sites) was measured, an 80% level was
138 observed for the WT as well as lines expressing only subunits, consistent with the activation
139 state typically observed for maize (Figure 3C; 23). In the three transgenic lines accumulating
140 more Rubisco enzyme, however, activation was reduced to 62-68%. However, a statistically
141 significant reduction in activation compared to WT was only observed in the UBI-SS-RAF1 line.
142 Regression analysis demonstrated a strong negative correlation between Rubisco content and
143 activation state (r^2=0.92, Figure 2d), indicating that not all of the additional Rubisco was being
144 activated. Yet, immunoblot analyses showed no major differences in Rubisco activase protein
145 abundance between the transgenic lines, or in comparison to WT (Figure S3). In order to
146 determine the amount of active Rubisco in each transgenic line we calculated *in vitro* V_{cmax} [%
147 active Rubisco (activation) x # of Rubisco active sites (content) x 5.5 (kcat; 5)]. These
148 calculations revealed that UBI-SS-RAF1 and UBI-LSSS-RAF1 may contain more active Rubisco

149 than WT, UBI-RAF1, UBI-SS or UBI-LSSS (54-56 μmol m^{-2} s^{-1} vs. 43-51 μmol m^{-2} s^{-1}; Table 1),
150 although this was not significant at $P<0.05$.

151 Plant height and fresh weight are increased in lines overexpressing RAF1 with Rubisco subunits
152 In order to evaluate the physiological effect of increased Rubisco in maize we conducted gas
153 exchange analysis, and used height and weight as proxies for any changes in plant growth rate.
154 In keeping with the modestly higher amounts of active Rubisco in UBI-SS-RAF1 and UBI-LSSS-
155 RAF1, as represented by *in vitro* V_{cmax}, leaf CO_2 assimilation rates trended higher at saturating
156 light and various CO_2 concentrations, especially for UBI-LSSS-RAF1 (Figures 3a and b). At light
157 saturated photosynthetic capacity ($A_{SAT,}$ 400 μl/L CO_2), UBI-LSSS-RAF1 showed a significant
158 increase of approximately 15% relative to WT (A_{SAT}, Table 1). When *in vitro* V_{cmax} was compared
159 to the maximum light-saturated rate of photosynthesis ($A_{SAT,}$ 400 μl/L CO_2), a positive correlation
160 was observed (r^2=0.78, Figure 3c), while Rubisco content and A_{SAT} did not show a significant
161 correlation (r^2=0.54, Figure 3d). This difference is likely due to a large portion of excess Rubisco
162 not being active and therefore not contributing to increases in photosynthesis.

163 Both UBI-SS-RAF1 and UBI-LSSS-RAF1 exhibited significantly increased height (Figures 4a
164 and 4b) and fresh weight (Figure 4c), while UBI-SS-RAF1 also showed increased dry weight
165 (Figure 4d). A comparison between A_{SAT} and above-ground fresh weight also revealed a strong
166 correlation (r^2=0.85, Figure 4e), suggesting the additional CO_2 being fixed is contributing to
167 enhanced growth.

168 Plants grown under greenhouse conditions showed the same trends as seen in the growth
169 chamber experiments (Figure S4). Both UBI-LSSS and UBI-LSSS-RAF1 showed significant
170 increases in CO_2 assimilation rates pre- and post-pollination (Figure S4a). Both genotypes also
171 showed significant increases in mature plant height (Figure S4b) and above ground dry weight
172 at maturity (Figure S4c). In addition, time to pollen production and silk production was
173 significantly reduced by two and 3-4 days respectively in the UBI-LSSS and UBI-LSSS-RAF1
174 genotypes relative to WT (Figures S4d-e).

175 Increased Rubisco activity does not shift the balance between C_3 and C_4 cycles
176 To assess whether increased Rubisco activity would disturb the balance between the C_3 and C_4
177 cycles, through the C_3 cycle's failure to compensate for increased flux through Rubisco, we
178 measured *in vitro* enzyme activities and *in vivo* BS leakiness. To test this, we first measured
179 PEPC and NADP-ME enzyme activities *in vitro* (Table 1). No significant differences were
180 observed in PEPC or NADP-ME activity, although NADP-ME activity correlated positively with
181 Rubisco activity (r^2=0.82, Figure 5a), unlike PEPC activity (Figure 5b). Next, we calculated the
182 PEPC/Rubisco and NADP-ME/Rubisco activity ratios (Table 1). No change was observed for
183 the NADP-ME/Rubisco activity ratio, whereas the PEPC/Rubisco activity ratio decreased
184 significantly in transgenic lines with the highest Rubisco activity, UBI-RAF1 and UBI-LSSS-
185 RAF1. To examine the C_3 vs C_4 cycle balance *in vivo* we estimated Φ from carbon isotope
186 discrimination, defined as the relative difference between ^{13}C:^{12}C in the photosynthetic product
187 relative to the ratio in CO_2 surrounding the leaf (24). No significant differences in Φ were
188 observed; suggesting the balance between the C_3 and C_4 cycles was not significantly perturbed
189 (Figure 5c).

Discussion

This study demonstrates the ability to increase Rubisco content and activity in a C_4 plant through altering the expression of a Rubisco assembly factor alone or along with Rubisco subunits. The overexpression of RAF1 appears to be the most important contributor to increasing Rubisco content in our plants. Rubisco content has previously been increased in rice, a C_3 plant, through the overexpression of *RBCS*, suggesting that SS availability limits Rubisco assembly (10). Increased Rubisco content, however, was not correlated with increased CO_2 assimilation, under a variety of test conditions. This could be ascribed in part to reduced activation, as well as other unidentified factors. In maize, overexpression of *RBCS* (or *RBCS* and *rbcL*) did not lead to increased Rubisco content (11), a result that was overcome here by simultaneously overexpressing the assembly chaperone RAF1, yielding up to 36% more Rubisco content (Figure 1b). This observation, along with the fact that overexpressing RAF1 alone positively impacted Rubisco activity (Figure 2a), reinforces the key role of RAF1 in Rubisco biogenesis, and suggests that Raf1, and likely BSD2, act as chaperone partners that protect the LS, possibly also the SS, from rapid proteolysis, which has been previously observed in mutants unable to express one or the other subunit (e.g. 25, 26, 27).

Though overexpression of LS and SS alone does not increase Rubisco content, there does appear to be a benefit with regards to plant growth and photosynthesis, which is most prominent under greenhouse conditions (Figure S4). One possibility is that overexpressing the subunits is increasing the rate of Rubisco synthesis and driving more rapid assembly of the enzyme. A second possibility is that there is less failure to complete assembly, resulting in a slower turnover rate. In either case this could reduce the metabolic load on the plant which could lead to increased vigor.

Structural analysis using cyanobacterial components revealed a Rubisco assembly intermediate consisting of eight large subunits and four RAF1 dimers, which were then displaced by SS (18). The additional RAF1 in our transgenic lines is therefore likely to stabilize the holoenzyme, and/or recruit and stabilize subunits earlier in the assembly process. It has been argued that C_4 plants cannot accommodate more Rubisco due to the constraints imposed by its compartmentalization in BS cells (28). Our data, however, show that at least in maize, significant Rubisco increases are possible (Figure 1b). We have additionally shown in maize that BS chloroplast coverage (i.e. the relative cellular area occupied by chloroplasts) can be increased through overexpression of another Rubisco assembly chaperone, BSD2, without obvious deleterious consequences (29). Whether either of these traits, conferred by transgene expression, would offer advantages under field conditions, remains to be determined.

Our transgenes were driven by the non-cell type-specific ubiquitin promoter, which in principle could have led to ectopic accumulation of Rubisco in M cells, which is not a physiologically desirable outcome. However, all detectable Rubisco was in BS cells (Figure 1c), suggesting that M-localized Rubisco subunits are actively degraded, and probably fail to assemble. Of the factors known to be required for plant Rubisco assembly (16), M expression may still be lacking for RbcX, CPS2/CPN60α, and/or RAF2, the latter two of which accumulates predominantly in BS cells (30).

231 Antisense RNA-mediated reduction of Rubisco content in the C_4 plant *Flaveria bidentis* indicated
232 that Rubisco accounts for up to 70% of the light-saturated photosynthesis limitation at optimal
233 growth temperatures (28, 31). The >30% increase of Rubisco in BS cells allowed us to test
234 whether this trait would be beneficial in terms of CO_2 assimilation and plant growth. Gas
235 exchange showed 15% higher light-saturated CO_2 assimilation in UBI-LSSS-RAF1 plants,
236 correlating with an increase in active Rubisco, and significant increases in fresh weight and
237 plant height (Table 1, Figure 3c and 4e). Increases in photosynthesis were of lower magnitude
238 than the increase in protein content, due to an apparent limitation of Rubisco activase, as the
239 activation state decreased up to 23% (Figure 2c). This was further confirmed through linear
240 regression analysis that showed Rubisco content did not correlate with $A_{SAT,}$ while active
241 Rubisco content does (Figures 3c and 3d).

242 Studies have been performed in both C_3 and C_4 species in which the activase level was
243 reduced. These have shown a decrease in photosynthesis only after at least a 60% reduction in
244 RCA amount (reviewed in 32). Consequently, RCA abundance has not been thought to limit
245 Rubisco activity under normal growth conditions. On the other hand, all studies where increased
246 Rubisco was reported, also reported decreased Rubisco activation, consistent with an RCA
247 limitation when Rubisco content is increased (10, 33-35). However, RCA abundance did not
248 appear to change in the increased Rubisco lines, suggesting more RCA protein may be needed
249 in order to activate the extra Rubisco (Figure S3). If RCA protein abundance is limiting,
250 combining overexpression of RCA with increased Rubisco could increase the photosynthetic
251 potential of these plants. However, if the RCA limitation results from a feedback response as
252 downstream reactions become overloaded, addition of RCA overexpression to high Rubisco
253 lines might not further enhance CO_2 assimilation and plant growth, and other steps in carbon
254 assimilation would also need to be targeted. For example, coupling upregulation of PPDK to
255 existing and RCA traits might further increase net photosynthesis, as PPDK has been shown to
256 have the most control on photosynthetic flux after Rubisco under light-saturated conditions (3).
257 Activase itself is also prone to activity modulation in maize depending on environmental
258 conditions (36), and we cannot rule out the relevance of these mechanisms.

259 Increasing Rubisco content is a substantial nitrogen investment which could compete with other
260 nitrogen sinks, particularly in C_3 plants, and perhaps as a consequence did not generate a
261 photosynthetic advantage in rice. This may be less of a problem in C_4 plants such as maize,
262 where the proportional nitrogen investment in Rubisco is significantly lower. Additionally, the C_4
263 CCM provides a high CO_2 environment, which competitively inhibits oxygenase activity and
264 allows Rubisco in C_4 plants to operate close to maximal efficiency. We therefore speculate that
265 the significantly lower N investment in C_4 Rubisco, combined with the presence of a CCM, led to
266 the observed results in maize. While additional Rubisco may not provide an advantage under
267 some growth conditions, the Rubisco pool may also be thought of as N storage (37, 38) that can
268 be remobilized under stress conditions and/or during leaf senescence (6).

269 While we did not observe any growth penalty under optimal conditions, highly expressing
270 transgenes may negatively affect yield due to the increased metabolic load (39). On the other
271 hand, increased Rubisco content might be beneficial under stress conditions where low Rubisco
272 content in C_4 plants has been hypothesized to negatively affect plant performance. For

example, carbon assimilation in C_4 species typically responds very negatively to chilling conditions (40), which may be related to the reduced activity and abundance of Rubisco. In maize, carbon assimilation decreases >60% at 14°C, while Rubisco abundance decreases ≥40% (41-43) , indicating that Rubisco content may limit photosynthetic capacity at low temperatures. If so, the chilling sensitivity of C_4 species such as maize could be overcome by increasing Rubisco expression. Indeed, chilling-tolerant C_4 species like *Miscanthus* x *giganteus* maintain Rubisco content under chilling conditions (43), which helps to sustain carbon assimilation. However, any improvement in Rubisco activity needs to be matched by C_4 cycle activity in order to improve overall carbon assimilation.

In this study, carbon isotope discrimination was measured in parallel with photosynthetic gas exchange to assess the balance between these cycles *in vivo* (Figure 5c). Since bundle sheath leakiness (Φ) was found to be similar in the transgenic lines with increased net assimilation, compared to the non-transgenic control, the rates of both cycles appear to have increased in concert, suggesting that upregulation of Rubisco in the C_3 cycle may have a feedback control on the rate of the C_4 cycle. Alternatively, the small increases in assimilation observed may not be sufficient to measure an observable change in leakiness. Enzyme activity analysis showed no correlation between Rubisco (C_3) and PEPC (C_4) activities, and the PEPC:Rubisco activity ratio decreased in transgenic lines with increased Rubisco activity (Table 1). These results are consistent with previous work suggesting that PEPC activity does not affect leakiness (44). Interestingly, we observed a positive correlation between Rubisco and NADP-ME activities (Figure 5a), which is consistent with unchanged bundle sheath leakiness and suggests that NADP-ME activity was able to adjust to the increased Rubisco activity. Increased NADP-ME activity as a result of increasing Rubisco content may also be part of the feedback control mechanism on the C_4 cycle, since antisense reduction of NADP-ME in *Flaveria bidentis* directly affected the flux through the C_4 cycle (45). Together, these results show that the ability of the M to supply CO_2 to the BS did not prevent an increase in net photosynthesis, suggesting a coordination between mesophyll capacity and Rubisco activity.

Conclusions

We have demonstrated that increasing Rubisco content in maize can help improve CO_2 assimilation and plant growth under laboratory conditions. Our approach could potentially be improved by tweaking Rubisco assembly or activity, but photosynthesis is a systems-level process, meaning that the ultimate agronomic aim of optimizing photosynthesis in the context of resilient and high-yielding crops, will also rely on modifications to light harvesting, plant architecture, and other aspects of photosynthetic metabolism (31, 46-48). Combining this work with the knowledge gained from other studies altering native protein expression that resulted in similar improvements in plant performance could help accomplish these goals (49, 50).

Methods

Construct Generation and Maize Transformation

Each maize transgenic cassette was driven by the maize ubiquitin1 promoter and includes the *Nos* terminator. These were assembled along with the ORF of interest into pGEM T-easy and introduced into Hi-II maize using *Agrobacterium*-mediated transformation (51). Details of UBI-

314 SS and UBI-LSSS constructs and characterization of transgenic lines are described in
315 Wostrikoff et al. 2012 (11). The binary vector pPTN1063, referred to as UBI-RAF1, incorporates
316 the ubiquitin1 promoter from pUbiHCnos (11), the maize *RAF1* open reading frame and the *Nos*
317 terminator from pHCnos (11). The *RAF1* gene was PCR amplified from leaf genomic DNA with
318 primers SpeI-c235f (5'-TTACTAGTATGCTCTCCCTCTCCCAC-3') and ClaIc235r (5'-
319 CAATCGATTCAGTCCCACTCCTCGTC-3'). The UBI-RAF1 plasmid contained the *aadA*
320 streptomycin resistance gene for bacterial selection and the *nptII* kanamycin resistance gene for
321 plant selection. Expression was determined for three independent RAF1 T1 single-insertion
322 events received from the Plant Transformation Core Research Facility at the University of
323 Nebraska-Lincoln, using immunoblot analysis with the RAF1 antibody (Figure S1; 14). No
324 evidence for gene silencing was observed in subsequent generations or after genetic crosses.
325 Primers used to genotype for the UBI-SS transgene are ZmUbiSSF4 (5'-
326 GCCCTGCCTTCATACGCTAT-3') and ZmUbiSSR4 (5'-TGGGAATTGGGATGGGATGG-3').

327

328 **Plant Growth**

329 Seed was germinated in 6L pots of 1/3 metro mix and 2/3 turface calcined clay soil mix, and
330 fertilized three times per week until harvest. For growth chamber experiments, plants were
331 grown in control environment chambers (Conviron, BDW40) under 25ºC/16 hour days and
332 20ºC/8 hour nights at a light intensity of 500-600 µmol m^{-2} s^{-1} and relative humidity of 70%. 40
333 days after planting, plant height measurements were taken at the top of the whorl (red dots,
334 Figure 4A). Above-ground fresh and dry weights were measured after cutting the plant just
335 above the soil. Leaves and stems were dried at 40ºC for 2 weeks. For greenhouse experiments,
336 plants were grown in under natural illumination at 28ºC/25ºC day/night. Plant height was
337 measured at the leaf collar of the youngest fully expanded leaf. This was repeated weekly from
338 3-10 weeks after germination.

339 **Mesophyll and Bundle Sheath Isolation and Protein analysis**

340 M and BS isolations were performed on 1 – 2 g of leaf tissue isolated from at least 3 plants, as
341 previously described (52). The BS extraction was carried out entirely at 4°C to minimize
342 degradation. Protein was then isolated from the M and BS extracts as described below. Total
343 protein was extracted on an equal leaf area basis since there were no differences in leaf mass
344 per area between the lines (Table 1). Two to four hole punches of tissue were taken from the tip
345 of the third leaf as described (53). Protein was separated using 13% SDS-polyacrylamide gels
346 and transferred onto polyvinylidene difluoride membranes (Bio-Rad). Primary antibodies were
347 incubated overnight at 4°C in Tris-buffered saline plus 0.1% Tween-20. Antibodies used were
348 anti-LS (Agrisera), anti-ME (a kind gift of Dr. Timothy Nelson, formerly of Yale University), anti-
349 PEPC (Agrisera), anti-Cpn60 (a gift from Spencer Whitney, ANU) and anti-RAF1 (14).
350 Incubation with goat anti-rabbit IR dye 800 CW (LI-COR) secondary antibody was performed at
351 room temperature for 2 hr and blots were imaged using the LI-COR Odyssey Infrared Imaging
352 System. Gels that were not blotted were stained with 0.01% Coomassie Blue R-250 and also
353 imaged using the Odyssey. For Blue Native gel electrophoresis, total soluble proteins were
354 extracted as described below for Rubisco activation and content measurements. 80 µL of plant
355 extract and 20 µL of native loading dye (80% glycerol, 0.01% Bromophenol Blue) were
356 combined. 15 µL of protein were loaded on 4-16% bis-Tris 1-mm gels (Invitrogen), run in a cold

357 room at low voltage overnight, and transferred onto polyvinylidene difluoride membranes using
358 the XCell II™ Blot Module (Invitrogen). Primary antibodies were incubated overnight and
359 detected via chemiluminescence. Native gels that were not blotted were fixed with 50%
360 methanol, 5% acetic acid and 40% water for 45 minutes and stained with GelCode Blue
361 (Fisher).

362 **Leaf gas exchange analysis**

363 All gas exchange measurements were performed with a LI-6400XT gas exchange system
364 (LICOR Biosciences, Lincoln, NE, USA) on the youngest fully expanded leaves of 3 ½ week old
365 plants. Responses of the net CO_2 assimilation rate (*A*) to intercellular CO_2 concentration (C_i)
366 were measured at a leaf temperature of 25°C and a light intensity of 1800 µmol m^{-2} s^{-1}. After the
367 plant was acclimated to these conditions inside the LI-6400XT leaf chamber for at least 10
368 minutes and reached steady state gas exchange, the A/C_i curves were measured with a
369 sequence of reference CO_2 concentrations of 400, 1000, 750, 550, 400, 350, 300, 250, 200,
370 150, 100, 75, 50, and 400 µmol mol^{-1}. Responses of the net CO_2 assimilation rate (*A*) to
371 photosynthetic photon flux density (PPFD) were also measured using the Li-6400XT gas
372 exchange system. Plants were acclimated to a leaf temperature of 25°C, a CO_2 concentration of
373 400 µl/L and a light intensity of 1800 µmol m^{-2} s^{-1} until reaching steady state. Subsequently,
374 PPFD was varied from 1800 to 1400, 1000, 800, 600, 400, 200, 150, 125, 100, 75, 50, and 25
375 µmol m^{-2} s^{-1}. Data points were taken in sequential order, with an equilibration time of between
376 180 and 300 seconds at each CO_2 concentration or light intensity. In the greenhouse
377 experiment net CO_2 assimilation rate was measured at a CO_2 concentration of 400 µmol mol^{-1}, a
378 leaf temperature of 25°C and a light intensity of 1800 µmol m^{-2} s^{-1}.

379 **Enzyme activation and content measurements**

380 Following gas exchange measurements, replicate leaf samples (0.5 cm^2) were frozen in liquid
381 nitrogen and stored at -80°C. Soluble protein from each leaf disc was extracted in 1 mL of ice-
382 cold, N_2-sparged extraction buffer [(50 mM EPPS-NaOH, pH 8.0, 0.5 mM EDTA, 2 mM DTT, 1%
383 (v/v) plant protease inhibitor cocktail (Sigma-Aldrich) and 1% (w/v) PVPP)] with 5 mM $MgCl_2$
384 using 2 mL Wheaton glass homogenizers kept on ice (23). The lysate was centrifuged for 30
385 sec (16,000 x g, 4 °C) and 10 µL of the soluble protein was assayed for initial and total Rubisco
386 activities using an NADH-coupled spectrophotometric enzyme assay at 25°C (54). Rubisco
387 content was determined using 100 µL of soluble extract by ^{14}C-CABP binding, as previously
388 described (55). Soluble protein content was measured using a Coomassie dye assay (Pierce)
389 with BSA standards. Total NADP-ME activity was determined in a spectrophotometric coupled
390 NADP assay as described previously (56). Total PEPC activity was determined in a NADH-
391 coupled spectrophotometric assay as described previously (56, 57). Protein extraction was
392 performed using the buffer described above for Rubisco activation and content measurements.

393 **Carbon isotope discrimination (Δ^{13}C) and bundle sheath leakiness (φ)**

394 Carbon isotope discrimination (Δ^{13}C) was measured simultaneously with gas exchange as
395 described (58). The youngest fully expanded leaf was clamped in the cuvette of an open gas
396 exchange system (LI-6800 with 6 cm^2 cuvette with integrated fluorometer), with light intensity
397 set to 1800 µmol m^{-2} s^{-1}, leaf temperature controlled at 25°C, cuvette CO_2 at 400 µmol mol^{-1},
398 and pre-mixed gas cylinder containing 2% O_2 and 98% N_2 connected to the air inlet, applying

399 manufacturer corrections for O_2-sensitivity of the infra-red gas analyzers. The exhaust stream of
400 the sample and reference IRGA were connected to two parallel cryogenic CO_2 trapping and
401 purification lines under partial vacuum. After steady state gas exchange was reached, CO_2 was
402 collected for 5 min while gas exchange parameters were recorded. Carbon isotope composition
403 of collected CO_2 was analyzed on an Isotope Ratio Mass Spectrometer (SIRA series II, VG
404 Isotech, modified by Provac Ltd, Crewe, Cheshire, UK) and observed $\Delta^{13}C$ was derived
405 according to Evans *et al.* (59). Bundle sheath leakiness was subsequently calculated from gas
406 exchange parameters and $\Delta^{13}C$ according to equations in Von Caemmerer *et al.* (24), using a
407 mesophyll conductance value of 1.78 mol m^{-2} s^{-1} bar^{-1} [measured on maize by Barbour *et al.*
408 (60)], and assuming ternary corrections apply, bicarbonate and CO_2 in the mesophyll cytoplasm
409 are in isotopic equilibrium, and bundle sheath [CO_2] >> mesophyll [CO_2]. For a more detailed
410 description of these assumptions see Kromdijk *et al.* (61).

411 **Statistical analysis**

412 Jmp pro version 13.1.0 software was used to determine the statistical significance of the
413 differences observed between the WT and transgenic lines. One-way ANOVA with post-hoc
414 Tukey HSD tests were performed, where different lowercase letters indicate significant
415 differences (P <0.05). Correlations between data sets were evaluated using Pearson's
416 correlation coefficient. n = number of individual biological replicates.

417 **Data Availability**

418 The data generated and analyzed during this study are available from the corresponding author
419 on reasonable request. Raw data would include photosynthesis and enzyme activity analyses.

420

421 **ACKNOWLEDGMENTS.** We acknowledge Tom Clemente and Shirley Sato (University of
422 Nebraska-Lincoln) for assembling the final transformation constructs, performing maize
423 transformations, and providing seed from T0 lines. Dr. Tim Nelson is acknowledged for sharing
424 ME antibody. This research was supported by the Agriculture and Food Research Initiative from
425 the National Institute of Food and Agriculture, U.S. Department of Agriculture, under award
426 number 2016-67013-24464. Travel to the Australian National University was supported by the
427 Mario Einaudi Center for International Studies, International Research Travel Grant at Cornell
428 University. We thank Steve Long (Univ. Illinois) for helpful discussions and manuscript
429 suggestions. RES is funded by the ARC Centre of Excellence for Translational Photosynthesis
430 (CE140100015) and ARC DECRA (DE13010760).

431 **Author Contributions**

432 CS participated in all experiments and drafted manuscript; RS participated in experiments
433 shown in Figures 1, 2, 3, 5, Table 1; FAB participated in experiments shown in Figure 3 and
434 Table 1; JK participated in some experiments presented in Figure 5 and Table 1; VB
435 participated in experiments shown in Figure S3-S4. DS was responsible for project
436 management and finalization of data analysis and manuscript preparation.

437

438 **Competing interests**

The authors declare no competing interests.

Corresponding author

Correspondence to David B. Stern, ds28@cornell.edu

References

1. Sharwood RE (2017) Engineering chloroplasts to improve Rubisco catalysis: prospects for translating improvements into food and fiber crops. *New Phytol.* 213(2):494-510.
2. Hauser T, Popilka L, Hartl FU, & Hayer-Hartl M (2015) Role of auxiliary proteins in Rubisco biogenesis and function. *Nat. Plants* 1:15065.
3. Furbank RT*, et al.* (1997) Genetic manipulation of key photosynthetic enzymes in the C_4 plant *Flaveria bidentis*. *Func. Plant Biol.* 24(4):477-485.
4. Ghannoum O*, et al.* (2005) Faster Rubisco is the key to superior nitrogen-use efficiency in NADP-malic enzyme relative to NAD-malic enzyme C_4 grasses. *Plant Physiol.* 137(2):638-650.
5. Sharwood RE, Ghannoum O, & Whitney SM (2016) Prospects for improving CO_2 fixation in C3-crops through understanding C4-Rubisco biogenesis and catalytic diversity. *Curr Opin Plant Biol* 31:135-142.
6. Feller U, Anders I, & Mae T (2008) Rubiscolytics: fate of Rubisco after its enzymatic function in a cell is terminated. *J. Exp. Bot.* 59(7):1615-1624.
7. Farquhar G (1983) On the nature of carbon isotope discrimination in C_4 species. *Functional Plant Biol.* 10(2):205-226.
8. Furbank R, Jenkins C, & Hatch M (1990) C_4 photosynthesis—quantum requirement, C_4 acid overcycling and Q-cycle involvement. *Aust. J. Plant Physiol.* 17:1–7.
9. Bracher A, Whitney SM, Hartl FU, & Hayer-Hartl M (2017) Biogenesis and Metabolic Maintenance of Rubisco. *Annual review of plant biology* 68(1):29-60.
10. Suzuki Y*, et al.* (2007) Increased Rubisco content in transgenic rice transformed with the 'sense' *rbcS* gene. *Plant Cell Physiol.* 48(4):626-637.
11. Wostrikoff K, Clark A, Sato S, Clemente T, & Stern D (2012) Ectopic expression of rubisco subunits in maize mesophyll cells does not overcome barriers to cell type-specific accumulation. *Plant Physiol.* 160(1):419-432.
12. Barkan A (1993) Nuclear mutants of maize with defects in chloroplast polysome assembly have altered chloroplast RNA metabolism. *Plant Cell* 5:389-402.
13. Brutnell TP, Sawers RJ, Mant A, & Langdale JA (1999) BUNDLE SHEATH DEFECTIVE2, a novel protein required for post- translational regulation of the *rbcL* gene of maize. *Plant Cell* 11(5):849-864.
14. Feiz L*, et al.* (2012) Ribulose-1,5-Bis-Phosphate Carboxylase/Oxygenase Accumulation Factor1 is required for holoenzyme assembly in maize. *Plant Cell* 24:3435-3446.
15. Feiz L*, et al.* (2014) A protein with an inactive pterin-4a-carbinolamine dehydratase domain is required for Rubisco biogenesis in plants. *Plant J.* 80(5):862-869.
16. Aigner H*, et al.* (2017) Plant RuBisCo assembly in *E. coli* with five chloroplast chaperones including BSD2. *Science* 358:1272-1278.

483 17. Kolesinski P*, et al.* (2013) Insights into eukaryotic Rubisco assembly - crystal structures of
484 RbcX chaperones from *Arabidopsis thaliana*. *Biochim. Biophys. Acta* 1830(4):2899-2906.
485 18. Hauser T*, et al.* (2015) Structure and mechanism of the Rubisco-assembly chaperone Raf1.
486 *Nat. Struct. Mol. Biol.*
487 19. Whitney SM, Birch R, Kelso C, Beck JL, & Kapralov MV (2015) Improving recombinant
488 Rubisco biogenesis, plant photosynthesis and growth by coexpressing its ancillary RAF1
489 chaperone. *Proc. Natl. Acad. Sci. USA* 112(11):3564-3569.
490 20. Wheatley NM, Sundberg CD, Gidaniyan SD, Cascio D, & Yeates TO (2014) Structure and
491 Identification of a pterin dehydratase-like protein as a Ribulose-bisphosphate
492 Carboxylase/Oxygenase (RuBisCO) assembly factor in the alpha-carboxysome. *J. Biol.*
493 *Chem.* 289(11):7973-7981.
494 21. Bhat JY, Thieulin-Pardo G, Hartl FU, & Hayer-Hartl M (2017) Rubisco Activases: AAA+
495 Chaperones Adapted to Enzyme Repair. *Frontiers in Molecular Biosciences* 4(20).
496 22. Mueller-Cajar O (2017) The Diverse AAA+ Machines that Repair Inhibited Rubisco Active
497 Sites. *Frontiers in Molecular Biosciences* 4(31).
498 23. Sharwood RE, Sonawane BV, Ghannoum O, & Whitney SM (2016) Improved analysis of
499 C4 and C3 photosynthesis via refined *in vitro* assays of their carbon fixation biochemistry. *J.*
500 *Exp. Bot.* 67(10):3137-3148.
501 24. von Caemmerer S, Ghannoum O, Pengelly JJL, & Cousins AB (2014) Carbon isotope
502 discrimination as a tool to explore C_4 photosynthesis. *J. Exp. Bot.* 65(13):3459-3470.
503 25. Rodermel S, Haley J, Jiang CZ, Tsai CH, & Bogorad L (1996) A mechanism for
504 intergenomic integration: abundance of ribulose bisphosphate carboxylase small-subunit
505 protein influences the translation of the large-subunit mRNA. *Proc. Natl. Acad. Sci. USA.*
506 93(9):3881-3885.
507 26. Johnson X*, et al.* (2010) MRL1, a conserved pentatricopeptide repeat protein, is required for
508 stabilization of *rbcL* mRNA in *Chlamydomonas* and *Arabidopsis*. *Plant Cell*.
509 27. Kanevski I & Maliga P (1994) Relocation of the plastid *rbcL* gene to the nucleus yields
510 functional ribulose-1,5-bisphosphate carboxylase in tobacco chloroplasts. *Proc. Natl. Acad.*
511 *Sci. USA* 91:1969-1973.
512 28. Kubien DS, von Caemmerer S, Furbank RT, & Sage RF (2003) C_4 photosynthesis at low
513 temperature. A study using transgenic plants with reduced amounts of Rubisco. *Plant*
514 *Physiol.* 132(3):1577-1585.
515 29. Salesse-Smith C, Sharwood RE, Sakamoto W, & Stern DB (2017) The Rubisco chaperone
516 BSD2 may regulate chloroplast coverage in maize bundle sheath cells. *Plant Physiol*
517 175(4):1624-1633.
518 30. Friso G, Majeran W, Huang M, Sun Q, & van Wijk KJ (2010) Reconstruction of metabolic
519 pathways, protein expression and homeostasis machineries across maize bundle sheath
520 and mesophyll chloroplasts; large scale quantitative proteomics using the first maize
521 genome assembly. *Plant Physiol.*
522 31. von Caemmerer S & Furbank RT (2016) Strategies for improving C_4 photosynthesis. *Curr.*
523 *Opin. Plant Biol.* 31(Supplement C):125-134.
524 32. Carmo-Silva E, Scales JC, Madgwick PJ, & Parry MA (2015) Optimizing Rubisco and its
525 regulation for greater resource use efficiency. *Plant, cell & environment* 38(9):1817-1832.
526 33. Suzuki Y, Miyamoto T, Yoshizawa R, Mae T, & Makino A (2009) Rubisco content and
527 photosynthesis of leaves at different positions in transgenic rice with an overexpression of
528 *RBCS*. *Plant Cell Environ.* 32(4):417-427.
529 34. Ishikawa C, Hatanaka T, Misoo S, Miyake C, & Fukayama H (2011) Functional
530 incorporation of sorghum small subunit increases the catalytic turnover rate of Rubisco in
531 transgenic rice. *Plant Physiol.* 156(3):1603-1611.

35. Morita K, Hatanaka T, Misoo S, & Fukayama H (2014) Unusual small subunit that is not expressed in photosynthetic cells alters the catalytic properties of Rubisco in rice. *Plant Physiol.* 164(1):69-79.
36. Crafts-Brandner SJ & Salvucci ME (2002) Sensitivity of photosynthesis in a C_4 plant, maize, to heat stress. *Plant Physiol.* 129(4):1773-1780.
37. Millard P (1988) The accumulation and storage of nitrogen by herbaceous plants. *Plant, Cell & Environ.* 11(1):1-8.
38. Millard P & Grelet G-a (2010) Nitrogen storage and remobilization by trees: ecophysiological relevance in a changing world. *Tree Physiol.* 30(9):1083-1095.
39. Sweetlove LJ, Nielsen J, & Fernie AR (2017) Engineering central metabolism – a grand challenge for plant biologists. *The Plant Journal* 90(4):749-763.
40. Farooq M, Aziz T, Wahid A, Lee D, & Siddique KHM (2009) Chilling tolerance in maize: agronomic and physiological approaches. *Crop Pasture Sci.* 60(6):501-516.
41. Long SP (1983) C_4 photosynthesis at low temperatures. *Plant Cell Environ.* 6(4):345-363.
42. Wang D, Portis AR, Jr., Moose SP, & Long SP (2008) Cool C_4 photosynthesis: pyruvate Pi dikinase expression and activity corresponds to the exceptional cold tolerance of carbon assimilation in *Miscanthus x giganteus*. *Plant Physiol.* 148(1):557-567.
43. Naidu SL, Moose SP, AK AL-S, Raines CA, & Long SP (2003) Cold tolerance of C_4 photosynthesis in *Miscanthus* x *giganteus*: adaptation in amounts and sequence of C_4 photosynthetic enzymes. *Plant Physiol.* 132(3):1688-1697.
44. Cousins AB*, et al.* (2007) The role of phosphoenolpyruvate carboxylase during C_4 photosynthetic isotope exchange and stomatal conductance. *Plant Physiol.* 145(3):1006-1017.
45. Brown RH (1999) Agronomic implications of C_4 photosynthesis. *C_4 plant Biol.*:473-507.
46. Ort DR*, et al.* (2015) Redesigning photosynthesis to sustainably meet global food and bioenergy demand. *Proc. Natl Acad. Sci. USA* 112(28):8529-8536.
47. Niyogi KK (2017) Editorial overview: Physiology and metabolism: Light responses from photoreceptors to photosynthesis and photoprotection. *Curr. Opin. Plant Biol.* 37(Supplement C):iv-vi.
48. Sarlikioti V, De Visser PH, Buck-Sorlin G, & Marcelis L (2011) How plant architecture affects light absorption and photosynthesis in tomato: towards an ideotype for plant architecture using a functional–structural plant model. *Ann.f Bot.* 108(6):1065-1073.
49. Glowacka K*, et al.* (2018) Photosystem II Subunit S overexpression increases the efficiency of water use in a field-grown crop. *Nature communications* 9(1):868.
50. Feng L*, et al.* (2007) Overexpression of SBPase enhances photosynthesis against high temperature stress in transgenic rice plants. *Plant Cell Rep* 26(9):1635-1646.
51. Sattarzadeh A*, et al.* (2010) Transgenic maize lines with cell-type specific expression of fluorescent proteins in plastids. *Plant biotechnology journal* 8:112-125.
52. Markelz NH, Costich DE, & Brutnell TP (2003) Photomorphogenic responses in maize seedling development. *Plant Physiol.* 133(4):1578-1591.
53. Barkan A (1998) Approaches to investigating nuclear genes that function in chloroplast biogenesis in land plants. *Meths. Enzymol.* 297:38-57.
54. Lilley RM & Walker DA (1974) An improved spectrophotometric assay for ribulosebisphosphate carboxylase. *Biochim. Biophys. Acta* 358(1):226-229.
55. Sharwood RE, von Caemmerer S, Maliga P, & Whitney SM (2008) The catalytic properties of hybrid Rubisco comprising tobacco small and sunflower large subunits mirror the kinetically equivalent source Rubiscos and can support tobacco growth. *Plant Physiol.* 146(1):83-96.
56. Ashton AR, Burnell JN, Furbank RT, Jenkins CLD, & Hatch MD (1990) Enzymes of C_4 Photosynthesis. *Methods in Plant Biochemistry*, ed Lea PJ (Academic Press Ltd, London), Vol 3, pp 39-71.

583 57. Sharwood RE, Sonawane BV, & Ghannoum O (2014) Photosynthetic flexibility in maize
584 exposed to salinity and shade. *J. Exp. Bot.* 65:3715-3724.
585 58. Kromdijk J, Griffiths H, & Schepers HE (2010) Can the progressive increase of C_4 bundle
586 sheath leakiness at low PFD be explained by incomplete suppression of photorespiration?
587 *Plant Cell Environ.* 33(11):1935-1948.
588 59. Evans J, Sharkey T, Berry J, & Farquhar G (1986) Carbon isotope discrimination measured
589 concurrently with gas exchange to investigate CO_2 diffusion in leaves of higher plants.
590 *Functional Plant Biol.* 13(2):281-292.
591 60. Barbour MM, Evans JR, Simonin KA, & Caemmerer S (2016) Online CO_2 and H_2O oxygen
592 isotope fractionation allows estimation of mesophyll conductance in C_4 plants, and reveals
593 that mesophyll conductance decreases as leaves age in both C_4 and C_3 plants. *New Phytol.*
594 210(3):875-889.
595 61. Kromdijk J, Ubierna N, Cousins AB, & Griffiths H (2014) Bundle-sheath leakiness in C_4
596 photosynthesis: a careful balancing act between CO_2 concentration and assimilation. *J.*
597 *Exp. Bot.* 65(13):3443-3457.

598

599 **Figure Legends**

600 Fig. 1. Maize transformation constructs and analysis of Rubisco content, cell type expression
601 and assembly status. **(a)** Schematics of ubiquitin promoter-driven constructs introduced into
602 maize. $RBCL_N$ denotes nucleus-encoded LS, a codon optimized *rbcL* gene preceded by a
603 chloroplast transit peptide. The grey box represents a Flag epitope tag present in the $RBCL_N$
604 transgene. **(b)** Average Rubisco content in 2 ½ week-old leaves ± SE quantified by ^{14}C-CABP
605 binding (n= the number of individual plants used for measurements; WT=11, RAF1=9, SS=10,
606 LSSS=12, SS-RAF1=12, LSSS-RAF1=12). Different lowercase letters indicate significant
607 differences (P<0.05); one-way ANOVA Tukey HSD. **(c)** Soluble protein was isolated from M and
608 BS cell preparations and analyzed by immunoblotting using the antibodies indicated at left (n=3
609 biologically independent experiments). α-PEPC and α-ME (malic enzyme) were used as
610 controls for M and BS cell purity, respectively. **(d)** Protein was isolated under native conditions
611 from total leaf tissue and analyzed by immunoblotting using the antibodies indicated below (n=3
612 biologically independent experiments). α-LS recognizes endogenous and transgene encoded
613 Rubisco, while α-FLAG recognizes transgene-encoded Rubisco large subunit. α-RAF1
614 recognizes the endogenous and transgene-encoded chaperone. Rb marks the position of the
615 Rubisco holoenzyme. * marks a band that may contain the LS-chaperonin complex as seen in
616 Feiz et al. (2012).

617 Fig. 2. Rubisco activity and activation state, and relationship to Rubisco content. Measurements
618 were performed on soluble protein extracted from leaf tissue of 2½ week old plants. **(a)** Rubisco
619 activity was measured using NADH-linked spectrophotometric assays (n= the number of
620 individual plants used for measurements; WT=11, RAF1=9, SS=9, LSSS=11, SS-RAF1=11,
621 LSSS-RAF1=12). **(b)** Correlation between Rubisco activity and Rubisco content. **(c)** Rubisco
622 activation status was determined by dividing initial Rubisco activity by total Rubisco activity (n=
623 the number of individual plants used for measurements; WT=4, RAF1=4, SS=3, LSSS=3, SS-
624 RAF1=4, LSSS-RAF1=3). **(d)** Correlation between Rubisco activation and Rubisco content. The
625 solid lines represent linear regressions from the data points calculated using Pearson's

626 coefficient of correlation. All values are shown as the mean ± SE. Different lowercase letters
627 indicate significant differences (P<0.05); one-way ANOVA Tukey HSD.

628 Fig. 3. Photosynthetic performance of maize lines. CO_2 and light response curves were
629 measured on the youngest fully expanded leaves of 3½ week old plants at 25ºC, using leaf gas
630 exchange. **(a)** Photosynthetic light response (A-Q) curves at 400 µl/L CO_2, (n= the number of
631 individual plants used for measurements; WT=4, RAF1=5, SS=4, LSSS=4, SS-RAF1=3, LSSS-
632 RAF1=4).PPFD, photosynthetic photon flux density. **(b)** CO_2 response (A-Ci) curves at 1800
633 µmol m^{-2} s^{-1}, (n= the number of individual plants used for measurements; WT=5, RAF1=6,
634 SS=5, LSSS=6, SS-RAF1=6, LSSS-RAF1=6). Values are shown as the mean ± SE. **(c)**
635 Correlation between *in vitro* V_{cmax} and the maximum light-saturated rate of photosynthesis
636 (A_{SAT}). **(d)** Correlation between Rubisco content and $A_{SAT.}$ The solid lines represent linear
637 regressions from the data points calculated using Pearson's coefficient of correlation. Values
638 are shown as the mean ± SE. Plants were grown and analyzed as described in Methods.

639 Fig. 4. Growth analysis. **(a)** A representative plant for each genotype is pictured prior to harvest,
640 40 days after planting. The red dot indicates the top of the whorl, with the horizontal white line
641 as a reference. Note that the order of SS and RAF1 in panel **(a)** is different than the order in
642 panels **b-d**. **(b)** Plant height, **(c)** above-ground fresh weight and **(d)** dry weight were measured
643 for each genotype. Values are shown as the mean ±SE (n= the number of individual plants used
644 for measurements; WT=7, RAF1=6, SS=7, LSSS=6, SS-RAF1=7, LSSS-RAF1=7).Different
645 lowercase letters indicate significant differences (P<0.05); one-way ANOVA Tukey HSD. **(e)**
646 Correlation between fresh weight and A_{SAT}. The solid lines represent linear regressions from the
647 data points calculated using Pearson's coefficient of correlation. Plants were grown and
648 analyzed as described in Methods.

649 Fig. 5. Relationships between *in vitro* and *in vivo* C_4 and C_3 cycle photosynthetic parameters.
650 Enzyme activity measurements were performed on soluble protein extracted from leaf tissue of
651 2½ week-old plants. Correlations between **(a)** NADP-ME activity and **(b)** PEPC activity with
652 Rubisco activity. The solid lines represent linear regressions from the data points calculated
653 using Pearson's coefficient of correlation. **(c)** BS leakiness measurements on 4-week-old plants.
654 Values are shown as the mean ± SE (n= the number of individual plants used for
655 measurements; WT=6, RAF1=5, SS=5, LSSS=5, SS-RAF1=6, LSSS-RAF1=5).No significant
656 differences were observed (P<0.05); one-way ANOVA Tukey HSD.

657

658

659

660 Table 1. Summary of leaf gas exchange, plant growth and photosynthetic enzyme activity.

661

662 Data represents averages of at least three replicates ± SE. Statistical significance tests and
663 mean ranking were conducted using one way Tukey-Kramer HSD ANOVA tests. Values
664 followed by the same letter are not significantly different at the 5% level (P<0.05). Values
665 significantly different from WT at the 5% level are in bold.

Parameter	WT	RAF1	SS	LSSS	SS-RAF1	LSSS-RAF1
Leaf gas exchange						
A_{SAT} (μmol m^{-2} s^{-1})	30.7 ±0.74*ab*	32.0 ±0.54*abc*	28.8 ±1.63*a*	33.8 ±0.71*bc*	33.8 ±0.92*bc*	**35.5±0.52*c***
BS Leakiness, Φ	0.21 ±0.01*a*	0.19 ±0.01*a*	0.21 ±0.02*a*	0.20 ±0.01*a*	0.22 ±0.01*a*	0.20 ±0.01*a*
Plant growth traits						
Height (cm)	73.2 ±1.8*a*	80.7 ±1.5*abc*	74.4 ±4.0*ab*	83.2 ±0.68*abc*	**84.5 ±2.9*bc***	**86.2 ±2.5*c***
Fresh Weight (g)	230.5 ±12.3*ab*	281.2 ±18.7*bc*	209.3 ±10.9*a*	291.7 ±6.7*bc*	**300.0 ±18.7*c***	**293.6 ±15.8*c***
Dry Weight (g)	28.8 ±0.75*a*	32.3 ±1.3*ab*	27.6 ±0.84*a*	33.5 ±1.2*ab*	**37.5 ±2.6*b***	32.9 ±1.1*ab*
Leaf Mass per Area (g m^{-2})	128.6 ±4.6*a*	143.4 ±11.3*a*	121.0 ±4.9*a*	137.4 ±3.0*a*	144.0 ±5.2*a*	129.0 ±4.7*a*
Photosynthetic enzymes						
Rubisco Content (μmol sites m^{-2})	11.7 ±0.4*a*	13.8 ±0.7*ab*	11.3 ±0.6*a*	11.8 ±0.8*a*	**15.9 ±0.4*b***	**15.5 ±0.6*b***
% Rubisco Activation	81.8 ±2.7*a*	68.9 ±3.0*ab*	79.7 ±4.5*a*	76.3 ±5.3*ab*	**61.5 ±2.5*b***	66.9 ±2.7*ab*
in vitro V_{cmax} (μmol m^{-2} s^{-1})	48.1 ±3.4*a*	49.8 ±3.4*a*	43.3 ±4.3*a*	50.8 ±9.2*a*	56.4 ±2.4*a*	53.6 ±2.8*a*
Rubisco Activity (μmol m^{-2} s^{-1})	35.6 ±2.7*a*	**51.2 ±2.9*b***	36.5 ±3.1*a*	35.6 ±4.3*a*	48.6 ±3.9*ab*	**52.3 ±2.5*b***
PEPC Activity (μmol m^{-2} s^{-1})	241.3 ±17.1*a*	227.7 ±38.7*a*	247.4 ±14.1*a*	199.3 ±19.3*a*	244.4 ±26.4*a*	221.4 ±21.4*a*
NADP-ME Activity (μmol m^{-2} s^{-1})	74.3 ±3.1*ab*	82.2 ±5.9*ab*	76.8 ±7.4*ab*	68.9 ±3.1*b*	83.8 ±3.4*ab*	89.6 ±4.2*a*
PEPC/Rubisco	7.8 ±01.0*a*	**4.6 ±0.6*bc***	7.6 ±0.8*ab*	6.4 ±0.4*abc*	6.1 ±0.6*abc*	**4.5 ±0.4*c***
NADP-ME/Rubisco	2.4 ±0.2*a*	1.7 ±0.1*a*	2.2 ±0.1*a*	2.3 ±0.2*a*	2.1 ±0.1*a*	1.8 ±0.1*a*

666

667

668

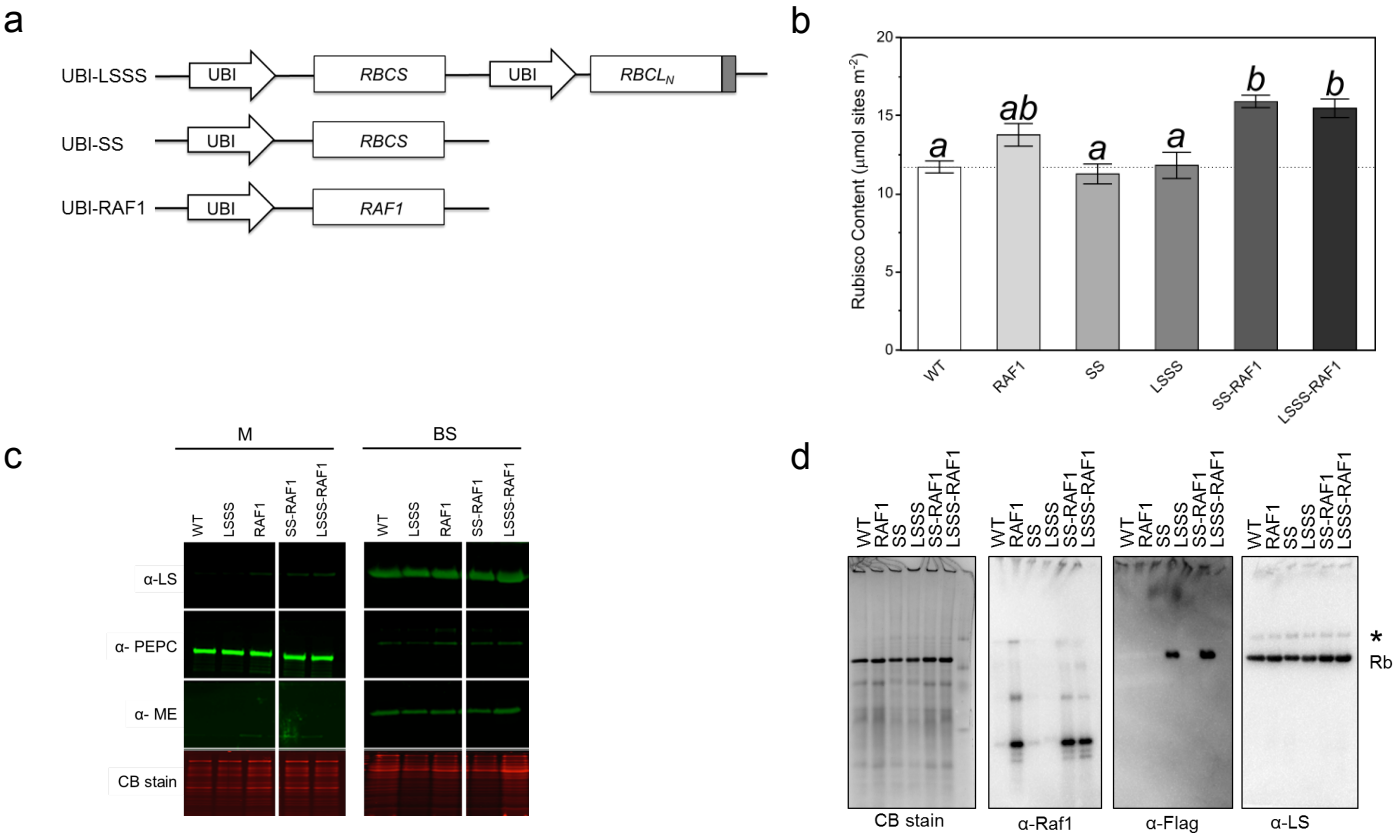

Fig. 1. Maize transformation constructs and analysis of Rubisco content, cell type expression and assembly status. **(a)** Schematics of ubiquitin promoter-driven constructs introduced into maize. *RBCL*$_N$ denotes nucleus-encoded LS, a codon optimized *rbcL* gene preceded by a chloroplast transit peptide. The grey box represents a Flag epitope tag present in the *RBCL*$_N$ transgene. **(b)** Average Rubisco content in 2 ½ week-old leaves ± SE quantified by ^{14}C-CABP binding (n= the number of individual plants used for measurements; WT=11, RAF1=9, SS=10, LSSS=12, SS-RAF1=12, LSSS-RAF1=12). Different lowercase letters indicate significant differences (P<0.05); one-way ANOVA Tukey HSD. **(c)** Soluble protein was isolated from M and BS cell preparations and analyzed by immunoblotting using the antibodies indicated at left (n=3 biologically independent experiments). α-PEPC and α-ME (malic enzyme) were used as controls for M and BS cell purity, respectively. **(d)** Protein was isolated under native conditions from total leaf tissue and analyzed by immunoblotting using the antibodies indicated below (n=3 biologically independent experiments). α-LS recognizes endogenous and transgene encoded Rubisco, while α-FLAG recognizes transgene-encoded Rubisco large subunit. α-RAF1 recognizes the endogenous and transgene-encoded chaperone. Rb marks the position of the Rubisco holoenzyme. * marks a band that may contain LS-chaperonin complex as seen in Feiz et al. (2012).

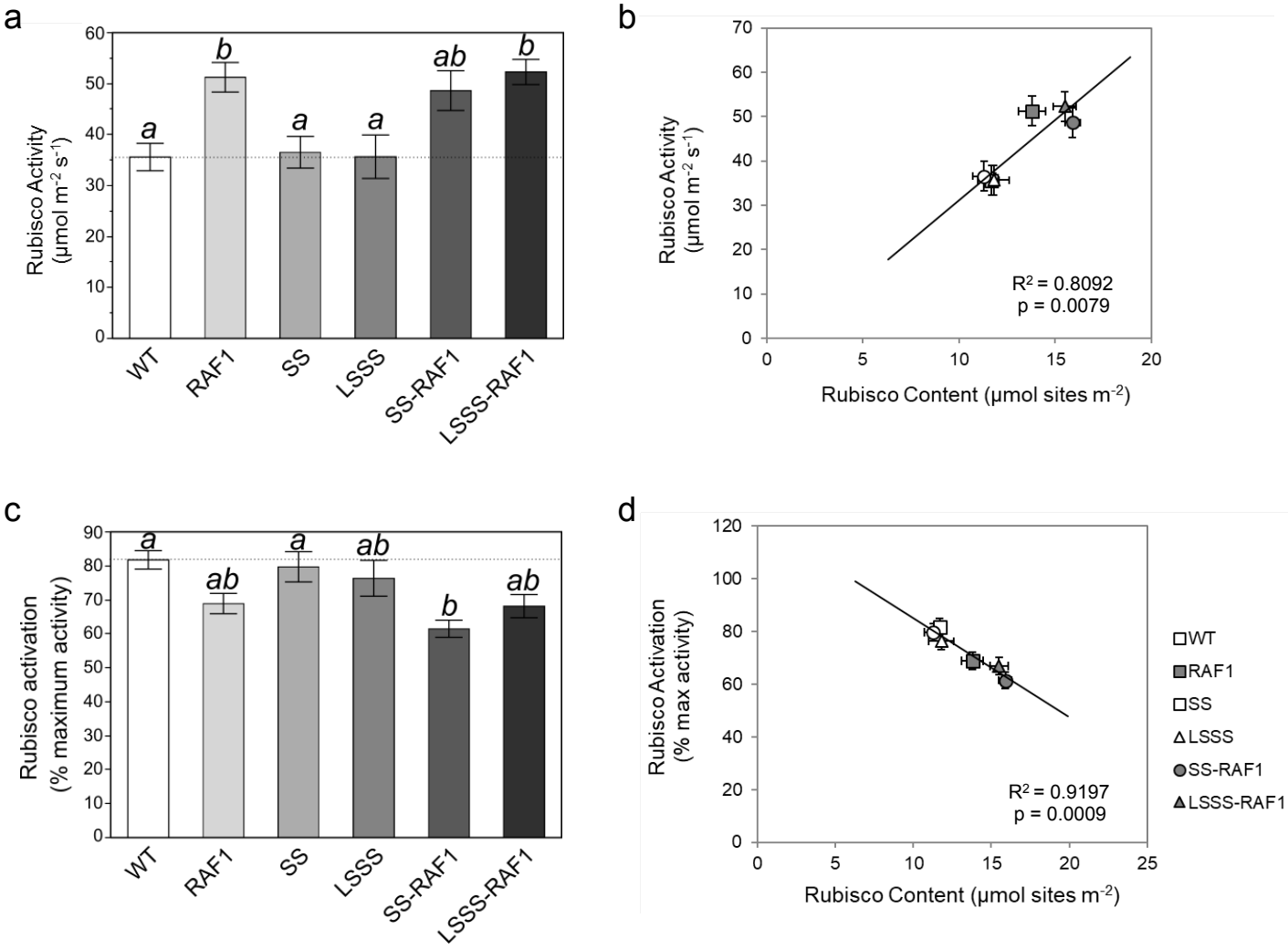

Fig. 2. Rubisco activity and activation state, and relationship to Rubisco content. Measurements were performed on soluble protein extracted from leaf tissue of 2½ week old plants. **(a)** Rubisco activity was measured using NADH-linked spectrophotometric assays (n= the number of individual plants used for measurements; WT=11, RAF1=9, SS=9, LSSS=11, SS-RAF1=11, LSSS-RAF1=12). **(b)** Correlation between Rubisco activity and Rubisco content. **(c)** Rubisco activation status was determined by dividing initial Rubisco activity by total Rubisco activity (n= the number of individual plants used for measurements; WT=4, RAF1=4, SS=3, LSSS=3, SS-RAF1=4, LSSS-RAF1=3). **(d)** Correlation between Rubisco activation and Rubisco content. The solid lines represent linear regressions from the data points calculated using Pearson's coefficient of correlation. All values are shown as the mean ± SE. Different lowercase letters indicate significant differences ($P<0.05$); one-way ANOVA Tukey HSD.

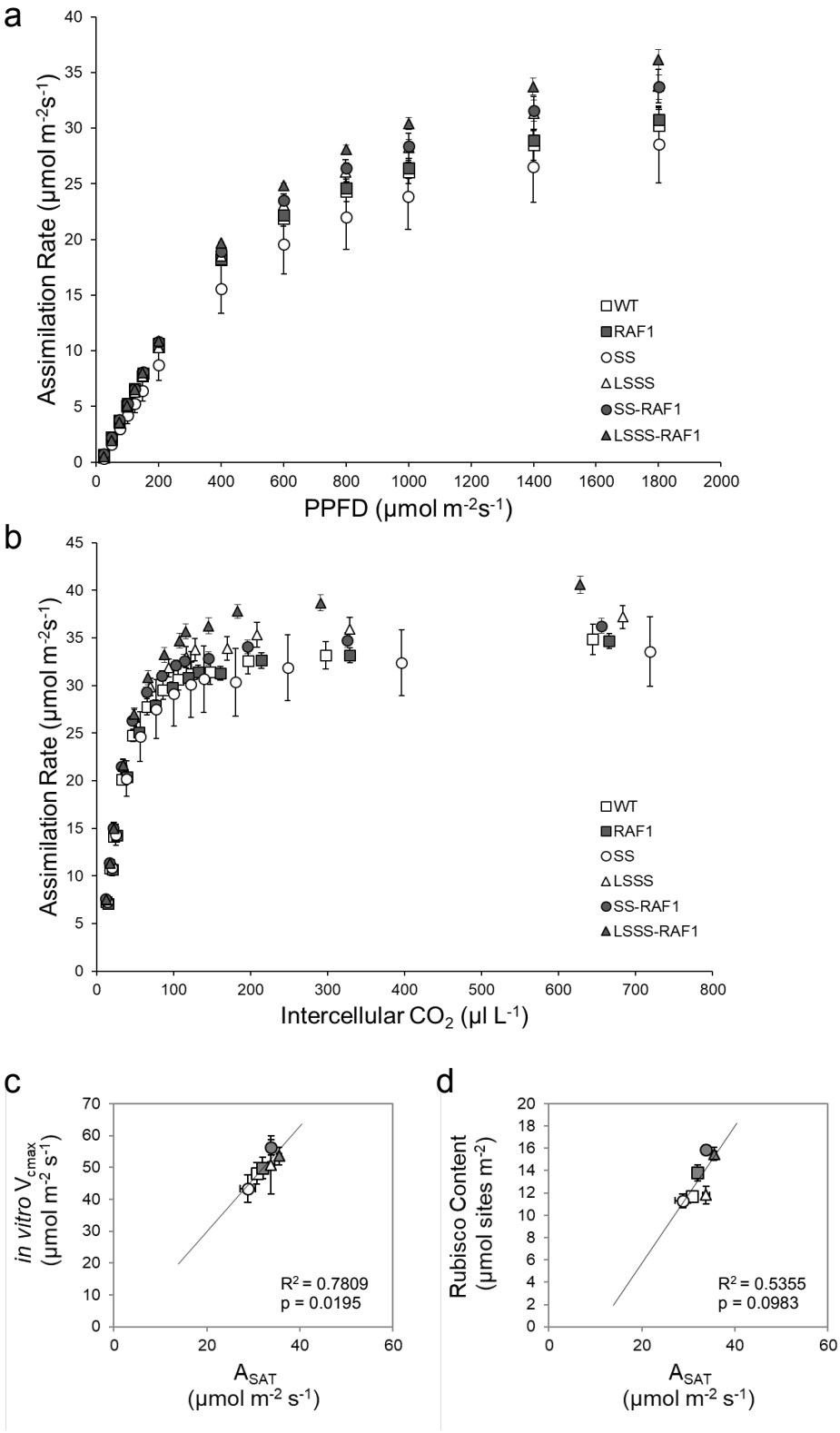
a
Assimilation Rate (µmol m-2s-1)
PPFD (µmol m-2s-1)
WT
RAF1
SS
LSSS
SS-RAF1
LSSS-RAF1
b
Assimilation Rate (µmol m-2s-1)
Intercellular CO2 (µl L-1)
WT
RAF1
SS
LSSS
SS-RAF1
LSSS-RAF1
c
in vitro Vcmax (µmol m-2 s-1)
ASAT (µmol m-2 s-1)
R2 = 0.7809
p = 0.0195
d
Rubisco Content (µmol sites m-2)
ASAT (µmol m-2 s-1)
R2 = 0.5355
p = 0.0983

Fig. 3. Photosynthetic performance of maize lines. CO_2 and light response curves were measured on the youngest fully expanded leaves of 3½ week old plants at 25ºC, using leaf gas exchange. **(a)** Photosynthetic light response (A-Q) curves at 400 µl/L CO_2, (n= the number of individual plants used for measurements; WT=4, RAF1=5, SS=4, LSSS=4, SS-RAF1=3, LSSS-RAF1=4). PPFD, photosynthetic photon flux density. **(b)** CO_2 response (A-Ci) curves at 1800 µmol m^{-2} s^{-1}, (n= the number of individual plants used for measurements; WT=5, RAF1=6, SS=5, LSSS=6, SS-RAF1=6, LSSS-RAF1=6). Values are shown as the mean ± SE. **(c)** Correlation between *in vitro* V_{cmax} and the maximum light-saturated rate of photosynthesis (A_{SAT}). **(d)** Correlation between Rubisco content and A_{SAT}. The solid lines represent linear regressions from the data points calculated using Pearson's coefficient of correlation. Values are shown as the mean ± SE. Plants were grown and analyzed as described in Methods.

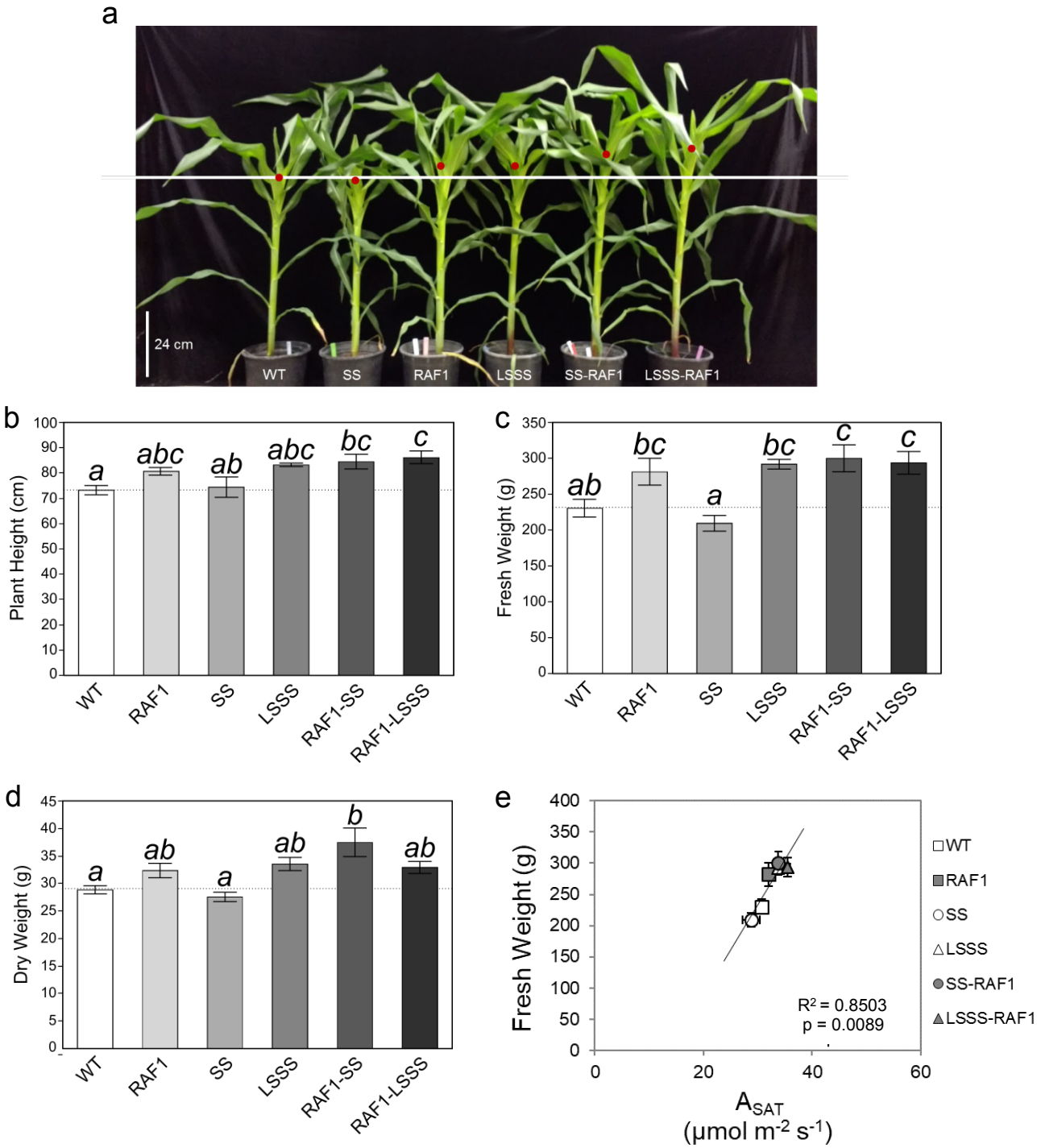
a
24 cm
WT
SS
RAF1
LSSS
SS-RAF1
LSSS-RAF1
b
Plant Height (cm)
a
abc
ab
abc
bc
c
WT
RAF1
SS
LSSS
RAF1-SS
RAF1-LSSS
c
Fresh Weight (g)
ab
bc
a
bc
c
c
d
Dry Weight (g)
a
ab
a
ab
b
ab
e
Fresh Weight (g)
R^2 = 0.8503
p = 0.0089
A_{SAT}
(μmol m^{-2} s^{-1})
WT
RAF1
SS
LSSS
SS-RAF1
LSSS-RAF1

Fig. 4. Growth analysis. **(a)** A representative plant for each genotype is pictured prior to harvest, 40 days after planting. The red dot indicates the top of the whorl, with the horizontal white line as a reference. Note that the order of SS and RAF1 in panel **(a)** is different than the order in panels **b-d**. **(b)** Plant height, **(c)** above-ground fresh weight and **(d)** dry weight were measured for each genotype. Values are shown as the mean ±SE (n= the number of individual plants used for measurements; WT=7, RAF1=6, SS=7, LSSS=6, SS-RAF1=7, LSSS-RAF1=7). Different lowercase letters indicate significant differences ($P<0.05$); one-way ANOVA Tukey HSD. **(e)** Correlation between fresh weight and A_{SAT}. The solid lines represent linear regressions from the data points calculated using Pearson's coefficient of correlation. Values are shown as the mean ±SE. Plants were grown and analyzed as described in Methods.

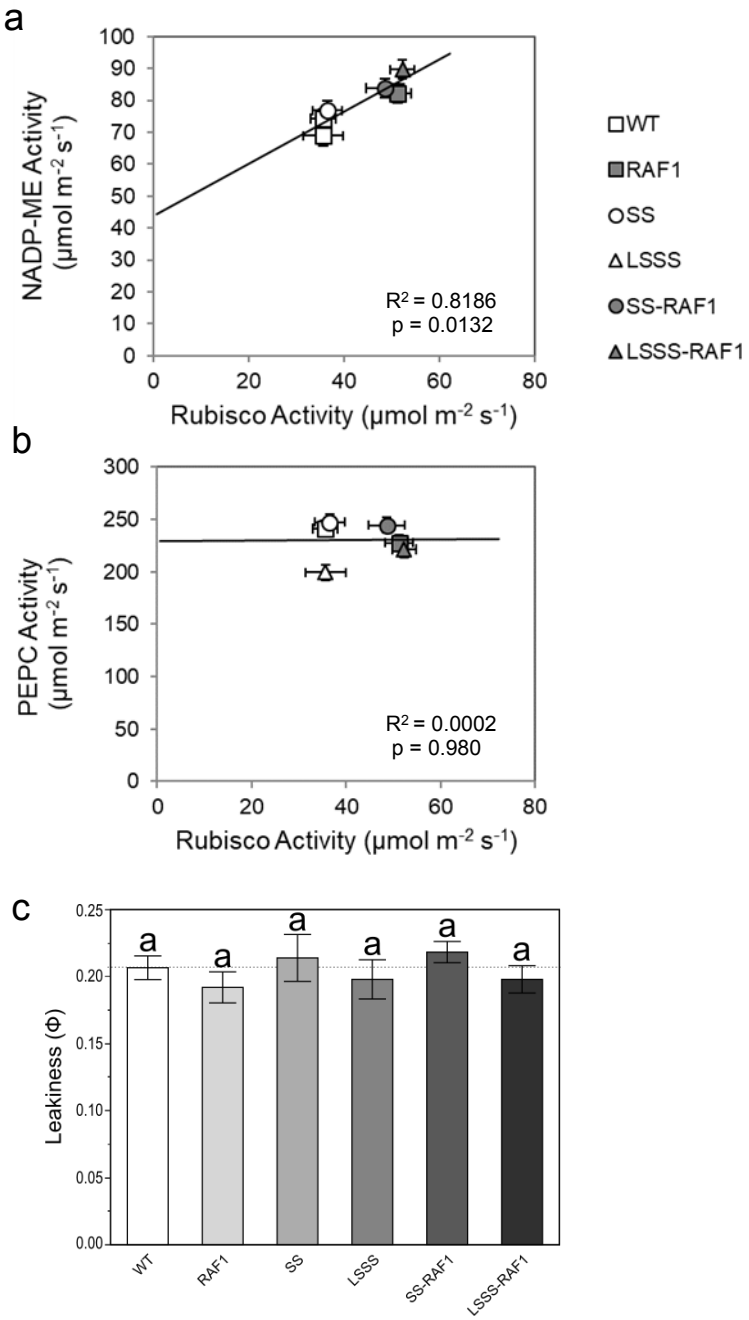

Fig. 5. Relationships between *in vitro* and *in vivo* C_4 and C_3 cycle photosynthetic parameters. Enzyme activity measurements were performed on soluble protein extracted from leaf tissue of 2½ week-old plants. Correlations between **(a)** NADP-ME activity and **(b)** PEPC activity with Rubisco activity. The solid lines represent linear regressions from the data points calculated using Pearson's coefficient of correlation. Values are shown as the mean ±SE. **(c)** BS leakiness measurements on 4-week-old plants. Values are shown as the mean ± SE (n= the number of individual plants used for measurements; WT=6, RAF1=5, SS=5, LSSS=5, SS-RAF1=6, LSSS-RAF1=5). Different lowercase letters indicate significant differences ($P<0.05$); one-way ANOVA Tukey HSD.

Table 1. Summary of leaf gas exchange, plant growth and photosynthetic enzyme activity.

Data represents averages of at least three replicates ± SE. Statistical significance tests and mean ranking were conducted using one way Tukey-Kramer HSD ANOVA tests. Values followed by the same letter are not significantly different at the 5% level (P<0.05). Values significantly different from WT at the 5% level are in bold.

Parameter	WT	RAF1	SS	LSSS	SS-RAF1	LSSS-RAF1
Leaf gas exchange						
A_{SAT} (μmol m^{-2} s^{-1})	30.7 ±0.74*ab*	32.0 ±0.54*abc*	28.8 ±1.63*a*	33.8 ±0.71*bc*	33.8 ±0.92*bc*	**35.5±0.52*c***
BS Leakiness, Φ	0.21 ±0.01*a*	0.19 ±0.01*a*	0.21 ±0.02*a*	0.20 ±0.01*a*	0.22 ±0.01*a*	0.20 ±0.01*a*
Plant growth traits						
Height (cm)	73.2 ±1.8*a*	80.7 ±1.5*abc*	74.4 ±4.0*ab*	83.2 ±0.68*abc*	**84.5 ±2.9*bc***	**86.2 ±2.5*c***
Fresh Weight (g)	230.5 ±12.3*ab*	281.2 ±18.7*bc*	209.3 ±10.9*a*	291.7 ±6.7*bc*	**300.0 ±18.7*c***	**293.6 ±15.8*c***
Dry Weight (g)	28.8 ±0.75*a*	32.3 ±1.3*ab*	27.6 ±0.84*a*	33.5 ±1.2*ab*	**37.5 ±2.6*b***	32.9 ±1.1*ab*
Leaf Mass per Area (g m^{-2})	128.6 ±4.6*a*	143.4 ±11.3*a*	121.0 ±4.9*a*	137.4 ±3.0*a*	144.0 ±5.2*a*	129.0 ±4.7*a*
Photosynthetic enzymes						
Rubisco Content (μmol sites m^{-2})	11.7 ±0.4*a*	13.8 ±0.7*ab*	11.3 ±0.6*a*	11.8 ±0.8*a*	**15.9 ±0.4*b***	**15.5 ±0.6*b***
% Rubisco Activation	81.8 ±2.7*a*	68.9 ±3.0*ab*	79.7 ±4.5*a*	76.3 ±5.3*ab*	**61.5 ±2.5*b***	66.9 ±2.7*ab*
in vitro V_{cmax} (μmol m^{-2} s^{-1})	48.1 ±3.4*a*	49.8 ±3.4*a*	43.3 ±4.3*a*	50.8 ±9.2*a*	56.4 ±2.4*a*	53.6 ±2.8*a*
Rubisco Activity (μmol m^{-2} s^{-1})	35.6 ±2.7*a*	**51.2 ±2.9*b***	36.5 ±3.1*a*	35.6 ±4.3*a*	48.6 ±3.9*ab*	**52.3 ±2.5*b***
PEPC Activity (μmol m^{-2} s^{-1})	241.3 ±17.1*a*	227.7 ±38.7*a*	247.4 ±14.1*a*	199.3 ±19.3*a*	244.4 ±26.4*a*	221.4 ±21.4*a*
NADP-ME Activity (μmol m^{-2} s^{-1})	74.3 ±3.1*ab*	82.2 ±5.9*ab*	76.8 ±7.4*ab*	68.9 ±3.1*b*	83.8 ±3.4*ab*	89.6 ±4.2*a*
PEPC/Rubisco	7.8 ±01.0*a*	**4.6 ±0.6*bc***	7.6 ±0.8*ab*	6.4 ±0.4*abc*	6.1 ±0.6*abc*	**4.5 ±0.4*c***
NADP-ME/Rubisco	2.4 ±0.2*a*	1.7 ±0.1*a*	2.2 ±0.1*a*	2.3 ±0.2*a*	2.1 ±0.1*a*	1.8 ±0.1*a*

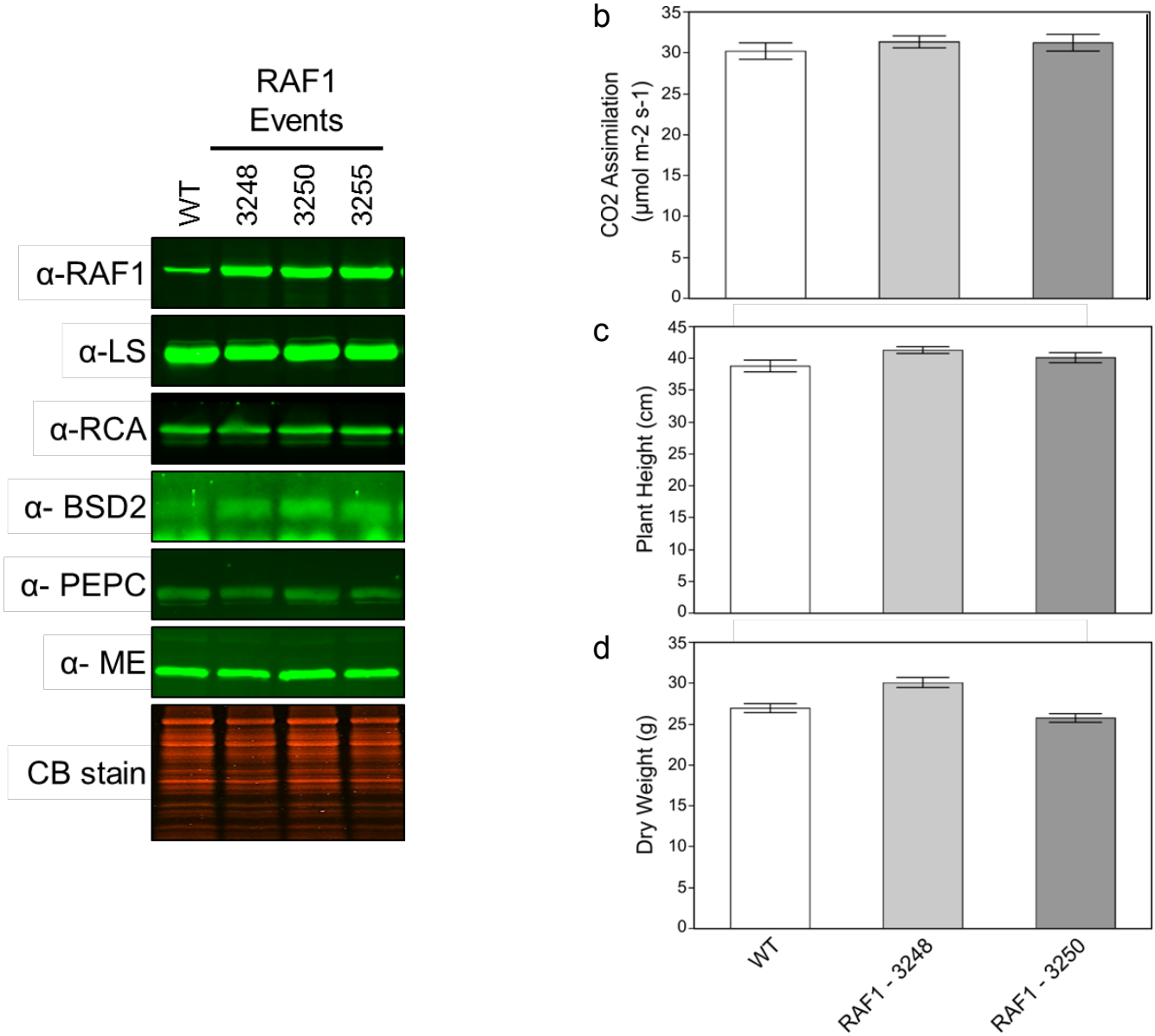

Fig. S1. Comparison of different RAF1 transgenic events. **(a)** Soluble protein was isolated on a leaf area basis from total leaf tissue of three transgenic events and analyzed by immunoblot (n=3 biologically independent experiments). **(b)** Light-saturated photosynthetic rate, **(c)** plant height and **(d)** dry weight were measured for two RAF1 transgenic events. Values are shown as the mean ± SE (n=5 biologically independent samples). No significant differences were observed (P<0.05); one-way ANOVA Tukey HSD.

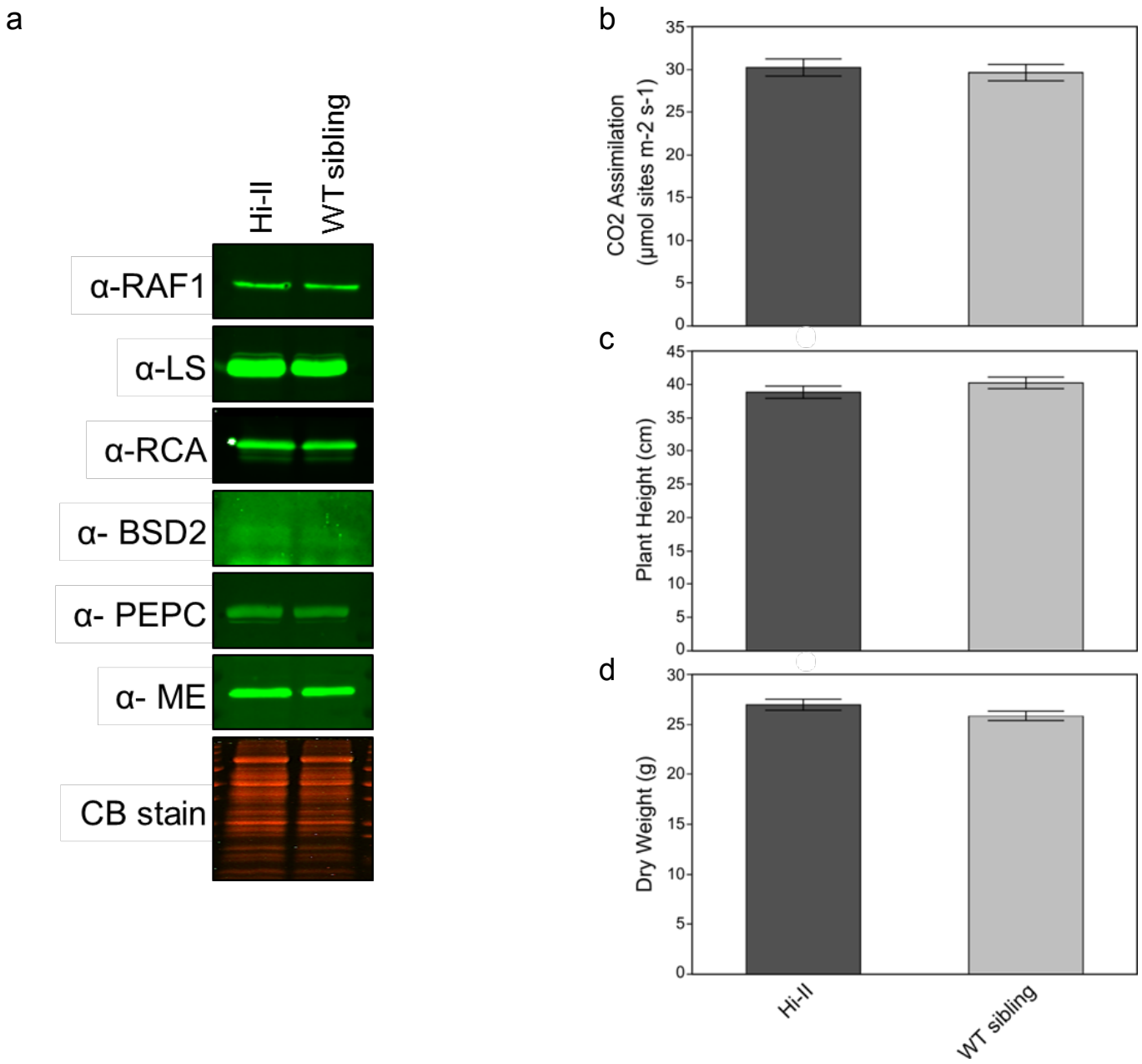

Fig. S2. Comparison of Hi-II WT controls and WT non-transgenic siblings used in this study. **(a)** Soluble protein was isolated on a leaf area basis from total leaf tissue of Hi-II and WT siblings and analyzed by immunoblot (n=3 biologically independent experiments). **(b)** Light-saturated photosynthetic rate, **(c)** plant height and **(d)** dry weight were compared. Values are shown as the mean ±SE (n=5 biologically independent samples). No significant differences were observed ($P<0.05$); one-way ANOVA Tukey HSD.

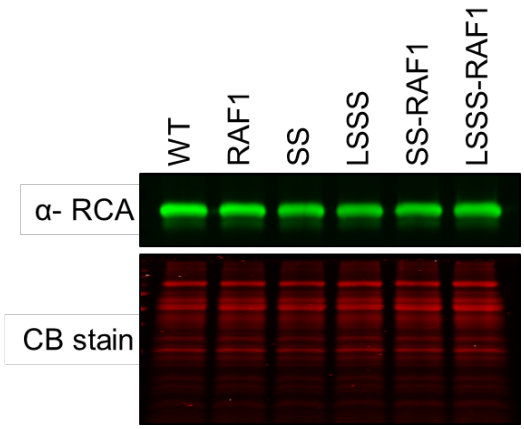

Fig. S3. Comparison of Rubisco activase expression between WT and transgenic lines. Soluble protein was extracted from leaf tissue of 2½ week-old plants on an equal leaf area basis and analyzed by immunoblotting using the Rubisco activase antibody, indicated at left (n=3 biologically independent experiments).

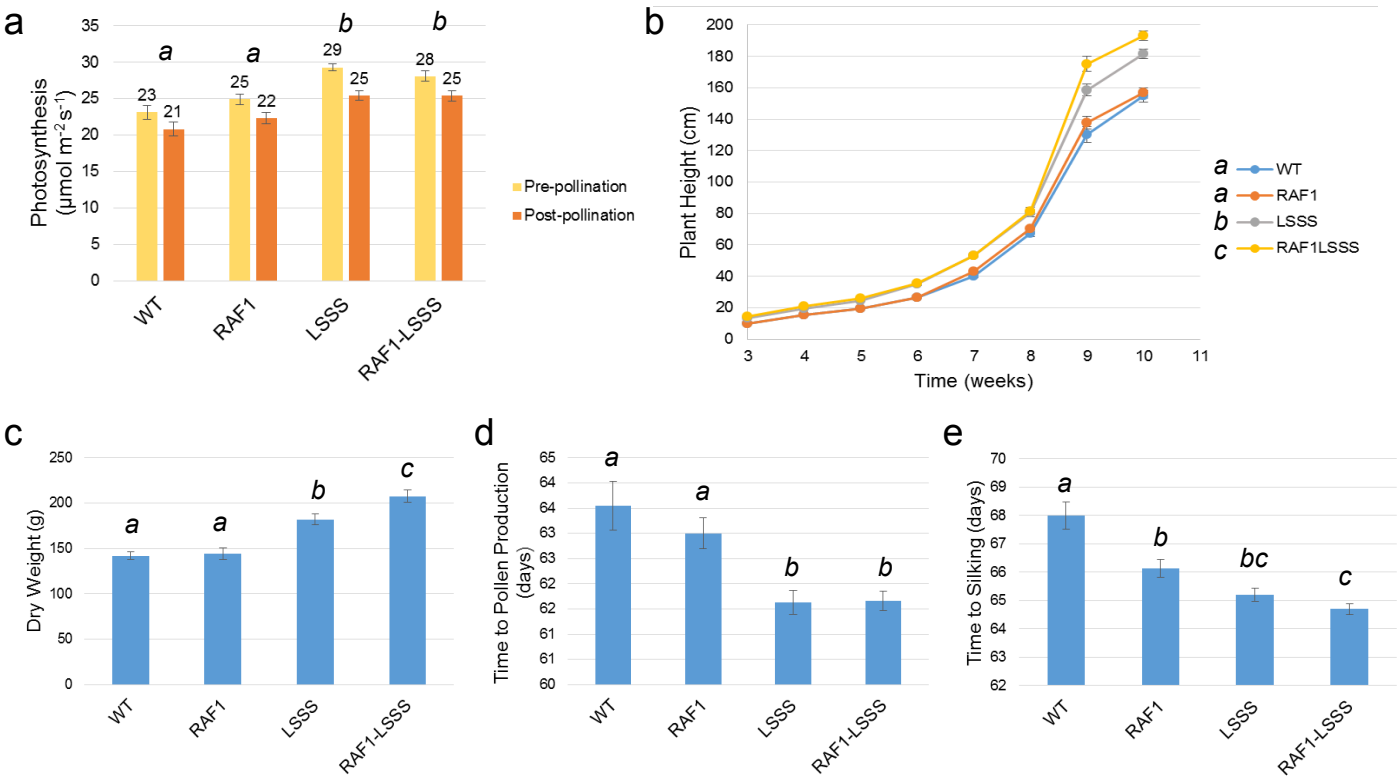

Fig. S4. Growth analysis under greenhouse conditions. **(a)** CO_2 assimilation rate pre-pollination (the day silks emerge, n= the number of individual plants used for measurements; WT=23, RAF1=28, LSSS=30, LSSS-RAF1=29) and post-pollination (2 weeks after silk emergence, n= the number of individual plants used for measurements; WT=20, RAF1=28, LSSS=30, LSSS-RAF1=29), **(b)** plant height over time (n= the number of individual plants used for measurements; WT=29, RAF1=29, LSSS=30 , LSSS-RAF1=30), **(c)** dry weight at maturity (n= the number of individual plants used for measurements; WT=28, RAF1=28, LSSS=30, LSSS-RAF1=29), **(d)** time to pollen production (n= the number of individual plants used for measurements; WT=29, RAF1=28, LSSS=30, LSSS-RAF1=30), and **(e)** time to silking (n= the number of individual plants used for measurements; WT=27, RAF1=29, LSSS=30, LSSS-RAF1=27) were measured for each genotype. Values are shown as the mean ±SE. Different lowercase letters indicate significant differences (P<0.05); one-way ANOVA Tukey HSD. The significance of the height measurement at 10 weeks is noted alongside the genotype legend.